

Quantum advantage for computations with limited space

Dmitri Maslov,¹ Jin-Sung Kim,² Sergey Bravyi,¹ Theodore J. Yoder,¹ and Sarah Sheldon²

¹*IBM Quantum, IBM T.J. Watson Research Center, Yorktown Heights, NY 10598, USA*

²*IBM Quantum, Almaden Research Center, San Jose, CA 95120, USA*

(Dated: May 3, 2022)

Quantum computations promise the ability to solve problems intractable in the classical setting. Restricting the types of computations considered often allows to establish a provable theoretical advantage by quantum computations, and later demonstrate it experimentally. In this paper, we consider space-restricted computations, where input is a read-only memory and only one (qu)bit can be computed on. We show that n -bit symmetric Boolean functions can be implemented exactly through the use of quantum signal processing as restricted space quantum computations using $O(n^2)$ gates, but some of them may only be evaluated with probability $\frac{1}{2} + \tilde{O}(\frac{1}{\sqrt{n}})$ by analogously defined classical computations. We experimentally demonstrate computations of 3- and a 4-bit symmetric Boolean functions by quantum circuits, leveraging custom two-qubit gates, with algorithmic success probability exceeding the best possible classically. This establishes and experimentally verifies a different kind of quantum advantage—one where a quantum bit stores more useful information for the purpose of computation than a classical bit. This suggests that in computations, quantum scrap space is more valuable than analogous classical space and calls for an in-depth exploration of space-time tradeoffs in quantum circuits.

Quantum computations are studied for their potential to offer an advantage over regular classical computations. The extent and provability of such advantage depend on the computational model selected. A simple example of a computational model can be a game. Consider the CHSH game [1] (Bell’s inequality [2]), where the two players Alice and Bob are given random Boolean inputs s and t and are required to come up with the bits a and b , respectively, and using no communication, such that $s \& t = a \oplus b$. The best classical probability of winning this game, $\frac{3}{4}$, can be improved to $\frac{2+\sqrt{2}}{4}$ with the use of a quantum computer. While this gap allows to experimentally demonstrate quantumness, there is very little quantum computation involved, and Bell’s inequality can be attributed to the property of quantum states rather than computations. A second model studies computations with black boxes. It allows proving computational complexity separations for a set of problems such as distinguishing constant and balanced functions (Deutsch-Jozsa [3]), discovering a hidden linear reversible function (BernsteinVazirani [4]), and finding a satisfying assignment (Grover [5]). While no practical utility is known for the first two problems/algorithms, Grover’s search can be employed to find a satisfying assignment for some complex but efficiently computable function. However, given a mere quadratic quantum speedup in a model that does not account for the cost of implementing the oracle, practical utilization of Grover’s search is likely far in the future. A third computational model studies white box computations, and allows superpolynomial advantage for solving problems such as Hamiltonian dynamics simulation [6–8] and discrete logarithm over Abelian groups (including Shor’s integer factoring [9]). In this case, separations are not established formally, although believed to hold, and a quantum computer capable of

outperforming a classical computer will likely need to be large—about 70 qubits and 650,000 gates in some of the shortest known post-classical quantum circuits [10] (the resource counts assume a perfect quantum computer, and are higher in the fault-tolerant scenario). Finally, a provable quantum advantage was established for the parallel model of computation. It was shown that parallel quantum algorithms can solve certain computational problems in constant time, whereas the best possible classical algorithm takes time growing at least logarithmically with the input size [11–16]. It remains to be seen whether this type of advantage can be demonstrated experimentally with near-term devices due to the large number of qubits required.

Here we study a simple computational model that allows to both establish a provable separation between classical and quantum computational models and validate it experimentally. Our model is designed to highlight the superiority of quantum computational space, resulting in a different type of advantage compared to those examples highlighted in the previous paragraph. A related space advantage should be possible to exploit to improve computations beyond those explicitly discussed in this paper.

Formally, we consider classical and quantum circuits where the primary input is a read-only memory (input cannot be written on), and the computational space is restricted to s bits. In the classical case, computations proceed by arbitrary $s+1$ -input s -output Boolean functions/gates g , where exactly one bit of the input to g is from the primary input, and all outputs are computational bits. For $s=1$ this means 2-input 1-output Boolean gates, being the staple gate library for classical computations. The closest analog to such transformations in the quantum world is the controlled- U gates, where the unitary operation U is applied to the computational register

and controlled by a primary input. We call this model limited-space computation.

The set of functions uncomputable by 1-bit limited-space classical computations includes symmetric functions $f(x) = f(x_1, x_2, \dots, x_n)$ taking different values when the Hamming weight of the input $|x| = x_1 + x_2 + \dots + x_n \in [2, n-1]$. This implies that most symmetric functions may not be computed classically in this model. However, they can be computed by a quantum circuit with $O(n^2)$ entangling gates and 1 qubit of computational space, as discussed later. Other than symmetric Boolean functions, polynomial-size 1-qubit limited-space quantum computations include at least those functions in the NC^1 class, such as Boolean components of the integer addition, integer multiplication, and matrix determinant [17]; most of these functions are uncomputable by 1-bit limited-space classical computations.

When the computational space is increased to 2 bits, the classical model can compute any Boolean function (e.g., by Disjunctive Normal Form). In this paper, we focus on the case $s=1$ to maximize the gap between classical and quantum computations.

With perfect quantum computers, we would be able to demonstrate that the quantum computer always succeeds at computing those functions uncomputable by the classical 1-bit limited-space circuits. Unfortunately, current quantum computers are noisy and sometimes fail. This failure is often modeled probabilistically. To demonstrate quantum advantage using noisy quantum computers over (perfect) classical computers in an experiment, it would be fair to arm classical computations with free access to randomness. Specifically, we allow the classical computer to randomly select a limited-space circuit to run or, equivalently, replace Boolean gates $g(x_i, s)$ in it with Boolean gates $g(x_i, s, r)$, where r is a random number. We furthermore allow the classical limited-space computer to evaluate functions with probability p , which is equal to the normalized distance of the truth vectors between the computable and desired function. The value p for classical computations is thus analogous to ASP (Algorithmic Success Probability) in quantum computations. Computational machinery that achieves ASP above the maximal classical value p performs a computation unreachable by classical means and is thereby superclassical. Here we demonstrate a selection of experiments that achieve this goal.

The simplest function not computable in the 1-bit limited-space classical model is MAJ3(x_1, x_2, x_3), the majority of three bits. In general, the majority is defined as $\text{MAJ}n(x_1, x_2, \dots, x_n) = 1$ iff $x_1 + x_2 + \dots + x_n > n/2$. The maximal classical probability p of computing MAJ3 using limited-space computations is $\frac{7}{8} = 0.875$, meaning the truth vector distance to a computable function is 1. We developed two quantum circuits to compute MAJ3, one with 8 entangling gates (Fig. 1(a)), achieved with the use of quantum signal processing, and one with 5 entan-

gling gates (Fig. 1(b)). The quantum computer ASPs are 0.9297 ± 0.0019 and 0.9481 ± 0.0020 for the 8 and 5 entangling gate circuits respectively, showing quantum advantage in both cases. For 4 qubits, the middle bit function MB4(x_1, x_2, x_3, x_4) computing the middle bit of the integer number $x_1 + x_2 + x_3 + x_4$ achieves the minimal among maximal classical values $p = \frac{13}{16} = 0.8125$ across all symmetric Boolean functions. We developed a quantum circuit with 7 entangling gates, Fig. 1(c), that maps into a quantum circuit with 13 entangling gates over the experiment, due to the requirement to use two SWAP gates. The measured ASP is 0.8655 ± 0.0094 , once again beating the classical threshold. For arbitrary n , $\text{MAJ}n(x_1, x_2, \dots, x_n)$ can be computed using $O(n^2)$ entangling gates by a quantum limited-space circuit, constructed using signal processing technique. In the Methods section we show that the classical probability p approaches $\frac{1}{2}$ for large n , namely, $p \leq \frac{1}{2} + O(\frac{\log n}{\sqrt{n}})$. This opens an opportunity to demonstrate larger quantum advantage with a higher number of qubits.

Our goal is the construction of a quantum circuit implementation of the n -bit Boolean function $f(x)$, expressed by an $n+1$ -qubit unitary $U : |x\rangle|b\rangle \rightarrow e^{i\theta(x,b)}|x\rangle|b \oplus f(x)\rangle$ for some real-valued function $\theta(x, b)$. In the 1-qubit limited-space model we may write $U = \sum_x |x\rangle\langle x| \otimes U(x)$, where $U(x)$ is the product of single-qubit gates, each controlled by a single qubit of the input register $|x\rangle$. We show in the Methods section that the simplest implementation of U in which $\theta(x, b)$ is constant and $U(x) = e^{i\theta(x,b)}X^{f(x)}$ is impossible. The closest we can get to such a phaseless implementation is $U(x) = (iX)^{f(x)}$, which we call a *true* implementation. Any other case we regard as a *relative phase* implementation. Note that both true and relative phase implementations faithfully compute $f(x)$ upon measurement in the computational basis. An advantage of true implementation comes from the ability to remove the phase entirely through introducing a new ancilla qubit.

Our structured approach to computing symmetric Boolean functions $f(x)$ makes use of quantum signal processing [8]. Suppose that we only access the input bits with a unitary $S = \sum_x |x\rangle\langle x| \otimes R_X(\phi_x)$, where $R_P(\chi) = \cos(\chi/2)I - i\sin(\chi/2)P$ is a single-qubit rotation for any Pauli operator $P \in \{X, Y, Z\}$. Letting $\phi_x = \Delta|x| - \delta$ for real parameters δ and Δ , it is clear that we can implement S with n controlled- $R_X(\Delta)$ gates and an $R_X(\delta)$ gate. Quantum signal processing is a method to create U using the S operation L times, interspersed with single-qubit gates on the computational qubit. In the simplest case, sufficient for our purposes, these additional single-qubit gates are Z -rotations $R_Z(\xi)$. To be more concrete, suppose we write $U(x) = A(x)I + iB(x)X + iC(x)Y + iD(x)Z$ for real-valued functions A, B, C , and D . Provided that these functions satisfy $A^2 + B^2 + C^2 + D^2 = 1$ and have certain symmetries, signal processing guarantees the existence of an-

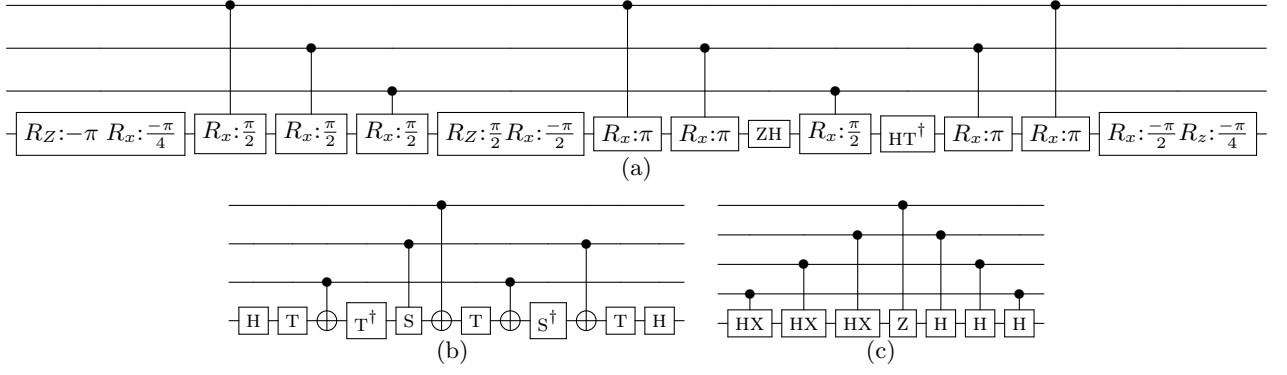


FIG. 1. (a) true MAJ3 with 8 entangling gates; (b) relative-phase MAJ3 with 5 entangling gates; (c) relative-phase MB4 with 7 entangling gates. The gates used are the Hadamard gate H , Pauli-Z gate Z , Phase gate S , T gate, CNOT gate, axial rotations $R_{\{x,y,z\}}:\theta$ by the angle θ , and controlled-HX, defined as the product of respective controlled- H and CNOT gates.

gles ξ_j such that $U = R_Z(\xi_0) \prod_{j=1}^L R_Z(\xi_j) S R_Z^\dagger(\xi_j)$ and gives an efficient method to find these angles [18, 19]. See the Methods section for more details.

To compute a symmetric function of n bits, we choose $A(x) = 1$ when $f(x) = 0$ and $B(x) = 1$ when $f(x) = 1$. For MAJ_n and when n is odd, these constraints are satisfiable for $L = 2n + 1$ uses of S (see Methods). Since each instance of S uses $n + 1$ gates, the total gate-complexity of this approach is $O(n^2)$. Circuit simplifications can reduce this gate count for specific solutions. For instance, the signal processing approach calculates true MAJ3 using 9 entangling gates, and a simple gate merging simplification reduces their number to 8, Fig. 1(a). The true 5-bit majority MAJ5 takes 25 entangling gates. For more general Boolean functions that lack certain symmetry present in MAJ_n , L may be required to be as large as $L = 4n + 1$. For instance, an unoptimized signal processing circuit for the true implementation of MB4 function takes 52 entangling gates. In contrast, a relative-phase implementation found by careful optimization has only 7 entangling gates, Fig. 1(c).

We implement the MAJ3 and MB4 functions in Qiskit [20], an open-source quantum software development platform, and execute the circuits on four or five fixed-frequency superconducting transmon qubits on *ibmq_berlin*, a 27-qubit heavy hexagonal lattice device [21] (Fig. 3 in the Methods section). For the MAJ3 function, qubits Q5, Q9, and Q11 are assigned as the read-only memory (ROM) inputs, while qubit Q8 is assigned as the ancilla (Fig. 2 insets). In this arrangement, each ROM input qubit is directly coupled to the ancilla qubit. For the MB4 function, qubit Q3 is included in the circuit as the fourth input. Qubit Q3 is only coupled to another ROM qubit, Q5, and not directly coupled to the ancilla qubit. As such, the states of Q3 and Q5 must be swapped twice during the execution of the MB4 circuit.

To execute these circuits efficiently, we calibrate a

custom two-qubit entangling gate and add single-qubit rotations to implement the following gates: $CNOT^{1/2}$, controlled-HX, and controlled-S. These gates are locally equivalent to a $ZX_{\pi/4}$ rotation, so while these gates can be implemented using two CNOT gates, the circuit length and overall performance is improved by calibrating and implementing a $ZX_{\pi/4}$ directly. In addition, we implement the two-qubit gates that are locally equivalent to CNOT, controlled-H and controlled-Z, using the single-qubit and CNOT gates included in Qiskit's gate set. These standard gates are automatically calibrated daily.

To calibrate the custom entangling gates, we utilize Qiskit Pulse [22, 23], a Qiskit module that allows the user to bypass the gate abstraction layer and implement controls directly at the microwave pulse level. Entangling gates between coupled qubits are achieved using an echoed cross-resonance (CR) microwave pulse in which a Gaussian-square shaped positive CR tone is applied to the control qubit at the target qubit's resonant frequency [24, 25]. A subsequent π pulse and negative CR tone applied to the control qubit echo away unwanted Hamiltonian terms [26]. The resulting interaction is primarily a ZX term which provides a conditional X rotation on the target qubit depending on the state of the control qubit.

A single echoed $ZX_{\pi/4}$ CR tone must be calibrated per ROM input to implement the custom gates, $CNOT^{1/2}$, controlled-HX, and controlled-S. Using Qiskit Pulse, we modify the length of the standard CNOT gate CR tone to roughly half the original duration, then recalibrate the amplitude to perform the $ZX_{\pi/4}$ rotation. In addition, a resonant 2π rotary echo is calibrated and applied to the target qubit simultaneously with the CR tone in order to minimize cross-talk between the target and spectator qubits [27]. After calibration, we assess the quality of these gates using randomized benchmarking [28], achieving $CNOT^{1/2}$ error rates of 0.00584 ± 0.00019 , 0.00351 ± 0.00014 , and 0.00339 ± 0.00013 for qubits Q5, Q11, and Q9, respectively. Details may be found in the

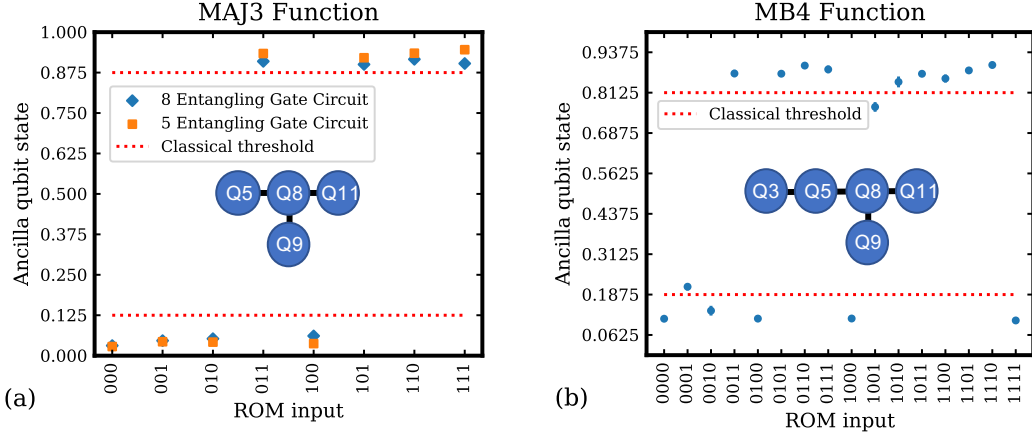


FIG. 2. Ancilla qubit (Q8) excited state population for each input ROM state combination for the (a) MAJ3 and (b) MB4 functions. The 5 and 8 entangling gate MAJ3 circuits achieve the ASP of 0.9481 ± 0.0020 and 0.9297 ± 0.0019 , while the MB4 circuit achieves the ASP of 0.8655 ± 0.0094 . The maximal classical ASP is illustrated with the red dotted lines. In addition, the qubit layout for each function is displayed in the inset of each plot.

Methods section.

The population of the ancilla qubit (Q8) in the Z-basis is shown in Fig. 2 for each input state for the MAJ3 and MB4 functions. We achieve the ASP of 0.9481 ± 0.0020 and 0.9297 ± 0.0019 for the 5 and 8 entangling gate MAJ3 circuits and 0.8655 ± 0.0094 for the MB4 circuit. Each of these results outperforms the corresponding maximal classical ASP of 0.875 and 0.8125 for the MAJ3 and MB4 functions, respectively. Each experiment was run with 8000 shots and repeated 100 times to build statistics for experimental error bars. As expected, the 5 entangling gate MAJ3 circuit outperforms the 8 entangling gate circuit, due to the shorter circuit length and fewer entangling gates. For the MB4 circuit, due to the connectivity restrictions of the device, the logical states of qubits Q3 and Q5 are swapped twice during the execution of the circuit to interact with the computational qubit Q8.

In this paper, we established the theoretical advantage of a certain kind of space-restricted quantum computations over analogously defined space-restricted classical computations and demonstrated it experimentally. Our experiment results in statistics that cannot be reproduced classically. Specifically, we demonstrated the calculation of 3- and 4-bit symmetric functions, relying on 1-qubit limited-space computations, with algorithmic success probabilities of 0.9481 ± 0.0020 and 0.8655 ± 0.0094 , beating the best possible classical statistics of 0.875 and 0.8215 respectively. The set of functions computable by 1-qubit limited-space quantum computations considered but not 1-bit limited-space classical computations includes functions such as the individual bits of the Hamming weight/popcount, a popular classical processor instruction, that is furthermore utilized in fault-tolerant implementations of certain Hamiltonian dynamics algorithms [10, 29]. Our study motivates further develop-

ment of space-restricted computations unique to quantum computers and an in-depth investigation of the space-time tradeoffs that appear to manifest very differently in the quantum compared to the classical worlds.

-
- [1] John F. Clauser, Michael A. Horne, Abner Shimony, and Richard A. Holt. Proposed experiment to test local hidden-variable theories. *Physical Review Letters*, 23(15):880, 1969.
 - [2] John S. Bell. On the Einstein Podolsky Rosen paradox. *Physics Physique Fizika*, 1(3):195, 1964.
 - [3] David Deutsch and Richard Jozsa. Rapid solution of problems by quantum computation. *Proceedings of the Royal Society of London. Series A: Mathematical and Physical Sciences*, 439(1907):553–558, 1992.
 - [4] Ethan Bernstein and Umesh Vazirani. Quantum complexity theory. *SIAM Journal on Computing*, 26(5):1411–1473, 1997.
 - [5] Lov K. Grover. A fast quantum mechanical algorithm for database search. In *Proceedings of the twenty-eighth annual ACM Symposium on Theory of Computing*, pages 212–219, 1996.
 - [6] Hale F. Trotter. On the product of semi-groups of operators. *Proceedings of the American Mathematical Society*, 10(4):545–551, 1959.
 - [7] Masuo Suzuki. Generalized Trotter’s formula and systematic approximants of exponential operators and inner derivations with applications to many-body problems. *Communications in Mathematical Physics*, 51(2):183–190, 1976.
 - [8] Guang Hao Low and Isaac L. Chuang. Optimal Hamiltonian simulation by quantum signal processing. *Physical Review Letters*, 118(1):010501, 2017.
 - [9] Peter W. Shor. Polynomial-time algorithms for prime factorization and discrete logarithms on a quantum computer. *SIAM Review*, 41(2):303–332, 1999.

- [10] Yunseong Nam and Dmitri Maslov. Low-cost quantum circuits for classically intractable instances of the Hamiltonian dynamics simulation problem. *npj Quantum Information*, 5(1):1–8, 2019.
- [11] Sergey Bravyi, David Gosset, and Robert König. Quantum advantage with shallow circuits. *Science*, 362(6412):308–311, 2018.
- [12] Sergey Bravyi, David Gosset, Robert König, and Marco Tomamichel. Quantum advantage with noisy shallow circuits. *Nature Physics*, pages 1–6, 2020.
- [13] François Le Gall. Average-case quantum advantage with shallow circuits. In *34th Computational Complexity Conference (CCC 2019)*. Schloss Dagstuhl-Leibniz-Zentrum fuer Informatik, 2019.
- [14] Matthew Coudron, Jalex Stark, and Thomas Vidick. Trading locality for time: certifiable randomness from low-depth circuits. *arXiv preprint arXiv:1810.04233*, 2018.
- [15] Adam Bene Watts, Robin Kothari, Luke Schaeffer, and Avishay Tal. Exponential separation between shallow quantum circuits and unbounded fan-in shallow classical circuits. In *Proceedings of the 51st Annual ACM SIGACT Symposium on Theory of Computing*, pages 515–526, 2019.
- [16] Daniel Grier and Luke Schaeffer. Interactive shallow Clifford circuits: quantum advantage against NC^1 and beyond. In *Proceedings of the 52nd Annual ACM SIGACT Symposium on Theory of Computing*, pages 875–888, 2020.
- [17] Farid Ablayev, Aida Gainutdinova, Marek Karpinski, Christopher Moore, and Christopher Pollett. On the computational power of probabilistic and quantum branching program. *Information and Computation*, 203(2):145–162, 2005.
- [18] Guang Hao Low, Theodore J. Yoder, and Isaac L. Chuang. Methodology of resonant equiangular composite quantum gates. *Physical Review X*, 6(4):041067, 2016.
- [19] Jeongwan Haah. Product decomposition of periodic functions in quantum signal processing. *Quantum*, 3:190, 2019.
- [20] Héctor Abraham and et al. Qiskit: An open-source framework for quantum computing, 2019.
- [21] Christopher Chamberland, Guanyu Zhu, Theodore J. Yoder, Jared B. Hertzberg, and Andrew W. Cross. Topological and subsystem codes on low-degree graphs with flag qubits. *arXiv preprint arXiv:1907.09528v2*, 2019.
- [22] Thomas Alexander, Naoki Kanazawa, Daniel J. Egger, Lauren Capelluto, Christopher J. Wood, Ali Javadi-Abhari, and David McKay. Qiskit pulse: Programming quantum computers through the cloud with pulses. *arXiv preprint arXiv:2004.06755*, 2020.
- [23] Shelly Garion, Naoki Kanazawa, Haggai Landa, David C. McKay, Sarah Sheldon, Andrew W. Cross, and Christopher J. Wood. Experimental implementation of non-Clifford interleaved randomized benchmarking with a controlled-S gate. *arXiv preprint arXiv:2007.08532*, 2020.
- [24] Chad Rigetti and Michel Devoret. Fully microwave-tunable universal gates in superconducting qubits with linear couplings and fixed transition frequencies. *Physical Review B*, 81(13):134507, 2010.
- [25] Jerry M. Chow, Antonio D. Córcoles, Jay M. Gambetta, Chad Rigetti, Blake R. Johnson, John A. Smolin, J. R. Rozen, George A. Keefe, Mary B. Rothwell, Mark B. Ketchen, and Matthias Steffen. Simple all-microwave entangling gate for fixed-frequency superconducting qubits. *Physical Review Letters*, 107(8):080502, 2011.
- [26] Sarah Sheldon, Easwar Magesan, Jerry M. Chow, and Jay M. Gambetta. Procedure for systematically tuning up crosstalk in the cross resonance gate. *Physical Review A*, 93(060302), 2016.
- [27] Neereja Sundaresan, Isaac Lauer, Emily Pritchett, Easwar Magesan, Petar Jurcevic, and Jay M. Gambetta. Reducing unitary and spectator errors in cross resonance with optimized rotary echoes. *arXiv preprint arXiv:2007.02925*, 2020.
- [28] Easwar Magesan, Jay M. Gambetta, and Joseph Emerson. Scalable and robust randomized benchmarking of quantum processes. *Physical Review Letters*, 106(18):180504, 2011.
- [29] Ian D. Kivlichan, Craig Gidney, Dominic W. Berry, Nathan Wiebe, Jarrod McClean, Wei Sun, Zhang Jiang, Nicholas Rubin, Austin Fowler, Alán Aspuru-Guzik, et al. Improved fault-tolerant quantum simulation of condensed-phase correlated electrons via trotterization. *Quantum*, 4:296, 2020.
- [30] Ryan O’Donnell. *Analysis of Boolean functions*. Cambridge University Press, 2014.
- [31] David C. McKay, Christopher J. Wood, Sarah Sheldon, Jerry M. Chow, and Jay M. Gambetta. Efficient Z gates for quantum computing. *Physical Review A*, 96:022330, 2011.

Acknowledgements. We thank Naoki Kanazawa and Edward Chen for experimental contributions and Jay M. Gambetta for discussions. S.B. and T.Y. are partially supported by the IBM Research Frontiers Institute.

METHODS

THEORY

The determinant constraint. Here we explain why the extra phase factor i in the definition of the quantum limited-space model is unavoidable. We examine the modified version of the model without the extra phase factor and argue that it is capable of computing only linear functions due to a certain determinant constraint.

Let $x \in \{0, 1\}^n$ be the input bit string and $V(x) = V_L(x) \cdots V_2(x)V_1(x)$, where each gate $V_i(x)$ is a single-qubit unitary operator that depends on at most one bit of x . Suppose $V(x)$ evaluates a Boolean function $f(x)$ such that

$$V(x)|b\rangle = |b \oplus f(x)\rangle \quad (1)$$

for all $x \in \{0, 1\}^n$ and $b \in \{0, 1\}$. We claim that this is possible only when $f(x)$ is a linear function. Indeed, Eq. (1) implies that $V(x) = X^{f(x)}$, where X is the Pauli- X operator. Since $\det(X) = -1$, one gets

$$(-1)^{f(x)} = \det(V(x)) = \prod_{j=1}^L \det(V_j(x)).$$

Suppose $V_j(x)$ depends on the bit $x_{a(j)}$, where $a(j) \in \{1, 2, \dots, n\}$. Then $\det(V_j(x)) = \exp[i\alpha_j + i\beta_j x_{a(j)}]$ for some real-valued coefficients α_j, β_j . We conclude that

$$\begin{aligned} (-1)^{f(x)} &= \prod_{j=1}^L e^{i\alpha_j + i\beta_j x_{a(j)}} \\ &= (-1)^{f(0^n)} \prod_{j=1}^L e^{i\beta_j x_{a(j)}} \\ &= (-1)^{f(0^n)} \prod_{p=1}^n \exp[i\gamma_p x_p], \end{aligned} \quad (2)$$

where γ_p is the sum of all coefficients β_j with $a(j)=p$. Let $e^p \in \{0, 1\}^n$ be a bit string with a single non-zero at the p -th bit. From Eq. (2) with $x=e^p$ one gets $e^{i\gamma_p} = (-1)^{f(e^p) + f(0^n)}$ and thus

$$f(x) = f(0^n) + \sum_{p=1}^n (f(e^p) + f(0^n))x_p \pmod{2}$$

for all x . Thus $f(x)$ is a linear function.

To enable computation of non-linear functions we introduce an extra phase factor in Eq. (1) such that

$$V(x)|b\rangle = \begin{cases} |b\rangle & \text{if } f(x) = 0, \\ i|b \oplus f(x)\rangle & \text{if } f(x) = 1. \end{cases}$$

In other words, $V(x) = (iX)^{f(x)}$. The determinant constraint no longer applies since $\det(V(x)) = 1$ for all x .

Classical no-go results. In this section, we examine the classical 1-bit limited-space model and characterize functions computable in this model. Recall that we consider n input bits $x = (x_1, x_2, \dots, x_n)$ stored in read-only memory and one ancilla bit that serves as a scratchpad. The ancilla is initialized in the state 0. At each computational step, it is allowed to examine a single input bit x_j and apply an arbitrary 1-bit gate to the ancilla. This gate may depend on the value of x_j . Such computation can be expressed by a program composed of elementary gates

$$\begin{aligned} \text{flip} &: \text{flip the ancilla,} \\ \text{reset}(c) &: \text{reset the ancilla to } c, \\ \text{flip}(j, b) &: \text{if } x_j = b \text{ then flip the ancilla,} \\ \text{reset}(j, b, c) &: \text{if } x_j = b \text{ then reset the ancilla to } c. \end{aligned}$$

Here $1 \leq j \leq n$ and $b, c \in \{0, 1\}$ are gate parameters. The program is said to compute a Boolean function $f(x)$ if the final state of the ancilla is $f(x)$ for all $x \in \{0, 1\}^n$. Let Ω_n be the set of all Boolean functions f with n input bits that can be computed by such programs. Note that no restrictions are imposed on the program length.

Here our goal is to quantify how well the n -bit Majority function MAJ_n can be approximated by functions from Ω_n . To this end, we develop an explicit characterization of Ω_n . First, we claim that any function $f \in \Omega_n$ can be computed by a simplified program that contains at most one gate $\text{reset}(j, b, c)$ for each $j \in \{1, 2, \dots, n\}$. Indeed, suppose the instruction $\text{reset}(j, b', c')$ appears before $\text{reset}(j, b, c)$. If $b' = b$, then removing $\text{reset}(j, b', c')$ does not change the function computed by the program. Specifically, if $x_j \neq b$, then none of the two gates is applied. If $x_j = b$, then both gates are applied but all computations that occurred before $\text{reset}(j, b, c)$ are irrelevant since the gate resets the ancilla. In the remaining case, when $b' \neq b$, one can replace $\text{reset}(j, b', c')$ by $\text{reset}(c')$. Indeed, if $x_j = b$, then all gates preceding $\text{reset}(j, b, c)$ can be ignored. Otherwise, if $x_j \neq b$, then $x_j = b'$ and thus $\text{reset}(j, b', c')$ is equivalent to $\text{reset}(c')$. This proves the claim.

Consider the simplified program discussed above. Let k be the total number of gates $\text{reset}(j, b, c)$. Choose the order of input variables x_j such that the program has the form $P_k, \text{reset}(k, b_k, c_k), \dots, P_2, \text{reset}(2, b_2, c_2), P_1, \text{reset}(1, b_1, c_1), P_0$. Here P_i are some programs composed of gates flip , $\text{reset}(c)$, $\text{flip}(j, b)$ only and b_i, c_i are some gate parameters. It is crucial that any program composed of gates flip , $\text{reset}(c)$, $\text{flip}(j, b)$ computes a linear function of x . Thus the full program computes a function $f(x)$ that becomes linear if we restrict the inputs x to one of the subsets

$$M_j = \{x : x_j = b_j \text{ and } x_i \neq b_i \text{ for } 1 \leq i < j\}$$

with $1 \leq j \leq k$ or

$$M_{k+1} = \{x : x_i \neq b_i \text{ for } 1 \leq i \leq k\}.$$

Indeed, if $x \in M_j$, then the tailing gates $\text{reset}(i, b_i, c_i)$ with $1 \leq i < j$ are not applied whereas the gate $\text{reset}(j, b_j, c_j)$ is applied. Thus all computations that occurred before $\text{reset}(j, b_j, c_j)$ are irrelevant. All computations that happen after $\text{reset}(j, b_j, c_j)$ are equivalent to the composition $P_{j-1} \cdots P_1 P_0$, which computes a linear function.

Note that restricting the function $f(x)$ to the subset M_j is equivalent to fixing the value for some j -tuple of variables. In particular, $f \in \Omega_n$ only if f can be made linear by choosing the value of a single variable x_j (restrict $f(x)$ to inputs $x \in M_1$). One can easily check that making any single variable of the Majority function $\text{MAJ}n$ be constant yields a non-linear function for $n \geq 3$. Thus $\text{MAJ}n \notin \Omega_n$. The same argument shows that the middle bit function $\text{MB4} \notin \Omega_4$. Indeed, fixing a single variable of MB4 yields a non-linear function $x_1 x_2 \oplus x_2 x_3 \oplus x_1 x_3$ or $x_1 x_2 \oplus x_2 x_3 \oplus x_1 x_3 \oplus x_1 \oplus x_2 \oplus x_3$.

How well can we approximate a given Boolean function $g: \{0, 1\}^n \rightarrow \{0, 1\}$ by a function $f \in \Omega_n$? Define an approximation ratio $R(g)$ as the maximum fraction of inputs $x \in \{0, 1\}^n$ such that $f(x) = g(x)$, where the maximum is taken over $f \in \Omega_n$. Note that $R(g) \geq 1/2$ since Ω_n includes both constant-valued functions. We claim that

$$R(g) \leq \frac{1}{2} [1 + \hat{g}_{\max} \log_2(4/\hat{g}_{\max})], \quad (3)$$

where $\hat{g}: \{0, 1\}^n \rightarrow \mathbb{R}$ is the binary Fourier transform of $g(x)$ defined as $\hat{g}(y) = 2^{-n} \sum_{x \in \{0, 1\}^n} (-1)^{x \cdot y + g(x)}$ and

$$\hat{g}_{\max} = \max_{y \in \{0, 1\}^n} |\hat{g}(y)|.$$

Indeed, let $f \in \Omega_n$ be the optimal approximation to g . Let $l_j: \{0, 1\}^n \rightarrow \{0, 1\}$ be a linear function such that $f(x) = l_j(x)$ for $x \in M_j$. Since the set of all n -bit strings is the disjoint union of the subsets M_1, M_2, \dots, M_{k+1} , one gets

$$R(g) = \sum_{j=1}^{k+1} \Pr[x \in M_j] \cdot \Pr[l_j(x) = g(x) | x \in M_j]. \quad (4)$$

Here and below the probability is taken over a random uniform $x \in \{0, 1\}^n$. Note that $\Pr[x \in M_j] = \frac{1}{2^j}$. By definition of the binary Fourier transform one has

$$\Pr[l(x) = g(x)] \leq \frac{1}{2} (1 + \hat{g}_{\max})$$

for any n -bit linear function $l(x)$ and thus

$$\Pr[l_j(x) = g(x) | x \in M_j] \leq \frac{1}{2} (1 + 2^j \hat{g}_{\max}). \quad (5)$$

Define $k_0 = \min\{k+1, \log_2(1/\hat{g}_{\max})\}$ and split the sum in Eq. (4) into two terms: those with $j \leq k_0$ and those with $j > k_0$. Using trivial bound

$\Pr[l_j(x) = g(x) | x \in M_j] \leq 1$ for $j > k_0$ and the bound in Eq. (5) for $j \leq k_0$ we arrive at

$$R(g) \leq \frac{1}{2} (1 + k_0 \hat{g}_{\max}) + \frac{1}{2^{k_0}}. \quad (6)$$

Furthermore, the term $\frac{1}{2^{k_0}}$ appears only if $k_0 < k+1$, in which case $k_0 = \log_2(1/\hat{g}_{\max})$ and $\frac{1}{2^{k_0}} = \hat{g}_{\max}$. Now Eq. (3) follows from Eq. (6). Let us point out that the bound Eq. (3) is tight up to the logarithmic factor. Indeed, it follows directly from the definitions that $R(g) \geq \frac{1}{2} (1 + \hat{g}_{\max})$.

It is known [30, Section 5.3] that the binary Fourier coefficients of $\text{MAJ}n$ have magnitude at most $\sqrt{2/\pi n}$. From Eq. (3) we conclude that

$$R(\text{MAJ}n) \leq \frac{1}{2} + O\left(\frac{\log(n)}{\sqrt{n}}\right).$$

In particular, $R(\text{MAJ}n) \approx \frac{1}{2}$ for large n , and thus $\text{MAJ}n$ is among the hardest functions to approximate by classical 1-bit limited-space computations. To obtain the exact value of $R(\text{MAJ}n)$ for small n we numerically computed a lookup table of all functions $f \in \Omega_n$. We found that $R(\text{MAJ}3) = \frac{7}{8}$, $R(\text{MB4}) = \frac{13}{16}$, and $R(\text{MAJ}5) = \frac{29}{32}$. We also calculated that $R(g) \geq \frac{7}{8}$ and $R(g) \geq \frac{13}{16}$ for any 3-bit and 4-bit Boolean functions g respectively. Thus $\text{MAJ}3$ and MB4 are the hardest functions to approximate of their respective size.

The above no-go results can be easily extended to probabilistic computations. Let $g: \{0, 1\}^n \rightarrow \{0, 1\}$ be a fixed Boolean function. Define an approximation ratio $R^*(g)$ as the maximum fraction of inputs $(x, r) \in \{0, 1\}^{n+m}$ such that $g(x) = f(x, r)$, where the maximum is taken over all integers $m \geq 0$ and over all functions $f \in \Omega_{n+m}$. Here $r \in \{0, 1\}^m$ represents a randomness consumed by the algorithm. We claim that $R^*(g) \leq R(g)$. Indeed, let $f_r(x) = f(x, r)$. Then $f_r \in \Omega_n$ for any fixed r . Thus the fraction of inputs x such that $f_r(x) = g(x)$ is at most $R(g)$ for any fixed r . By linearity, the fraction of inputs (x, r) such that $f(x, r) = g(x)$ is at most $R(g)$.

Quantum Signal Processing. Here we describe a scalable method to compute the Majority of n bits on a quantum computer using $O(n^2)$ two-qubit and $O(n)$ single-qubit gates.

Signal processing begins with a simple question [18]. *Question 1:* Suppose we fix a positive integer L . Can a given unitary $U(\phi)$ be written as

$$U(\phi) = R_Z(\xi_0) \prod_{j=1}^L R_Z(\xi_j) R_X(\phi) R_Z^\dagger(\xi_j), \quad (7)$$

for a selection of real numbers ξ_j , $j = 0, 1, \dots, L$? Notice that this is a question of functional equivalence—one has to construct $U(\phi)$ for *all* values of the “signal” ϕ , a real number.

We may always write $U(\phi) = A(\phi)I + iB(\phi)X + iC(\phi)Y + iD(\phi)Z$ for real-valued functions A, B, C , and D . In fact, because $R_X(\phi) = \frac{1}{2}e^{-i\phi/2}(I+X) + \frac{1}{2}e^{i\phi/2}(I-X)$, we see that A, B, C , and D are functions of $t = e^{i\phi/2}$. Indeed, they are Laurent polynomials in t with degree L . For example, $A(t) = \sum_{j=-L}^L a_j t^j$.

With this setup, we claim that Question 1 has an affirmative answer if and only if

- (i) $A(t)^2 + B(t)^2 + C(t)^2 + D(t)^2 = 1$.
- (ii) A, B, C , and D are Laurent polynomials of degree at most L , and at least one has degree L .
- (iii) Each A, B, C , and D is an even function if L is even and an odd function if L is odd.
- (iv) $A(t)$ and $D(t)$ are reciprocal functions, i.e. $A(t) = A(1/t)$. Similarly, $B(t)$ and $C(t)$ are anti-reciprocal, i.e. $B(t) = -B(1/t)$.

Reference [19] contains proof and an efficient algorithm to find the necessary angles ξ_j .

Often, signal processing is used to create a desired, complex behavior $U(\phi)$ when one can easily create the simple behavior $R_X(\phi)$. However, in certain situations, one would prefer not to have to specify all four functions A, B, C , and D . For our purposes, for example, only the behaviors of A and B matter. Thus, a second, complementary question is the following. *Question 2:* Given $A(t)$ and $B(t)$, do there exist functions $C(t)$ and $D(t)$ such that A, B, C , and D together satisfy the conditions (i-iv)?

Question 2 has an affirmative answer if and only if A and B are Laurent polynomials with the symmetries required by (ii-iv) and $0 \leq A(\phi)^2 + B(\phi)^2 \leq 1$ for all real ϕ . Moreover, the computation of angles ξ_j remains efficient [19].

We take these general principles of quantum signal processing and apply them to the computation of $\text{MAJ}_n(x)$. As described in the main text, we define $\phi_x = \Delta|x| - \delta$ for the input bit string $x \in \{0, 1\}^n$. For reasons soon to become clear, we choose $\Delta = \frac{2\pi}{n+1}$ and $\delta = \frac{\pi}{2} \frac{n-1}{n+1}$. This spaces the points of interest, ϕ_x for $|x| = 0, 1, \dots, n$, at and evenly between $\phi = -\delta$ and $\phi = \pi + \delta$. Then, our goal is the construction of U so that $U(\phi_x)$ equals I when $\text{MAJ}_n(x) = 0$ and equals iX when $\text{MAJ}_n(x) = 1$.

Achieving this goal requires the construction of A and B satisfying conditions (ii-iv), $0 \leq A(\phi)^2 + B(\phi)^2 \leq 1$, and

$$A(\phi_x) = \begin{cases} 0, & \text{MAJ}_n(x) = 1 \\ 1, & \text{MAJ}_n(x) = 0 \end{cases}, \quad (8)$$

$$B(\phi_x) = \begin{cases} 0, & \text{MAJ}_n(x) = 0 \\ 1, & \text{MAJ}_n(x) = 1 \end{cases}. \quad (9)$$

To argue later that $A(\phi)^2 + B(\phi)^2 \leq 1$ we also require

$$\frac{d}{d\phi} A(\phi_x) = 0 \quad \text{and} \quad \frac{d}{d\phi} B(\phi_x) = 0, \quad (10)$$

for all $x \in \{0, 1\}^n$.

We assume L is odd. This makes A an odd, reciprocal Laurent polynomial: $a_j = -a_{-j}$ for odd j , and $a_j = 0$ for even j . Our approach is to use the linear system of equations implied by Eqs. (8) and (10) to solve for a_1, a_3, \dots, a_L , a total of $(L+1)/2$ variables. Because $A(\phi) = A(-\phi) = -A(2\pi - \phi) = -A(-2\pi - \phi)$ and our choices of Δ and δ many of the equations end up automatically satisfied (e.g. $A(\pi) = 0$) or redundant (e.g. $A(-\delta) = A(\delta) = 1$). In the end, only $n+1$ equations remain. The requirement to have enough variables to obtain a solution implies $L \leq 2n+1$. This is not necessarily the equality only because we do not rule out other redundancies in the equations, though numerical calculations for small n have not found any. We choose $A(t)$ to be the minimum degree Laurent polynomial solving the linear system.

Similarly, B is an odd, anti-reciprocal Laurent polynomial. To simplify the problem, we can choose $B(t) = A(-it)$, which means that $B(\phi) = A(\phi)$ shifted by $\pi/2$. In fact, both $A(\phi)$ and $B(\phi)$ are non-negative for all $\phi \in [0, \pi]$.

Now we show that $P(\phi) = 1 - A(\phi)^2 - B(\phi)^2$ is never negative. Consider the sum $E(\phi) = A(\phi) + B(\phi)$, which equals one for all ϕ_x . Moreover, $E(\phi)$ does not equal one elsewhere because A and B are minimal degree Laurent polynomials satisfying the constraining equations above. Since $\frac{d}{d\phi} E(\phi_x) = 0$ for all x and $E(\phi) < 1$ for some value of $\phi \in [0, \pi]$, we see that $0 \leq E(\phi) \leq 1$ for all $\phi \in [0, \pi]$. By the symmetries of $A(\phi)$ and $B(\phi)$ noted previously this implies all the following:

$$\begin{aligned} A(\phi) + B(\phi) &\leq 1, \quad A(\phi)B(\phi) \geq 0, \quad \text{for } \phi \in [0, \pi], \\ A(\phi) - B(\phi) &\leq 1, \quad A(\phi)B(\phi) \leq 0, \quad \text{for } \phi \in [-\pi, 0], \\ -A(\phi) + B(\phi) &\leq 1, \quad A(\phi)B(\phi) \leq 0, \quad \text{for } \phi \in [\pi, 2\pi], \\ -A(\phi) - B(\phi) &\leq 1, \quad A(\phi)B(\phi) \geq 0, \quad \text{for } \phi \in [-2\pi, -\pi]. \end{aligned} \quad (11)$$

These together imply that $P(\phi) \geq 0$ for all ϕ . For instance, if $\phi \in [0, \pi]$, then $P(\phi) = 1 - (A(\phi) + B(\phi))^2 + 2A(\phi)B(\phi) \geq 0$. Similar arguments hold for the other three intervals.

With this, we completed the construction of U to compute the Majority. At most $2n+1$ uses of $R_X(\phi_x)$ are required. Each of these takes n two-qubit gates to implement, leading to a total of $O(n^2)$ two-qubit gates. Each application of $R_X(\phi_x)$ is also accompanied by a constant number of single-qubit gates, leading to a total of $O(n)$ single-qubit gates.

We note that sometimes not all the derivative constraints, Eq. (10), are necessary to guarantee $P(\phi) \geq 0$. For $n=3$ and $n=5$ we are able to find suitable A and B by only requiring zero derivatives where the functions evaluate to one—a feat impossible for $n=7$. Moreover, significant simplification may occur when it happens that the consecutive angles ξ_j and ξ_{j+1} are equal. In this case, subsequent R_Z gates in Eq. (7) cancel and two

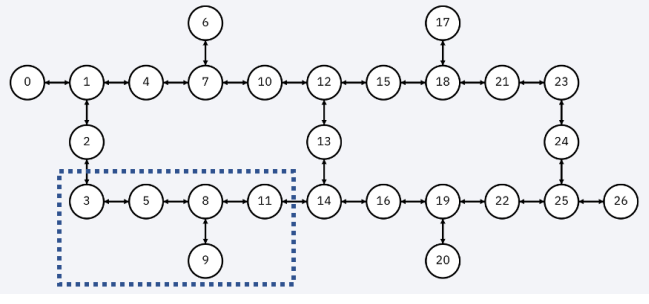


FIG. 3. Connectivity diagram of *ibmq_berlin* with the qubits used in the experiment highlighted.

$R_X(\phi_x)$ rotations can be combined into a $R_X(2\phi_x)$ gate, which needs just n two-qubit gates, rather than $2n$, to implement. Hence, we obtain smaller than anticipated circuits—a circuit with 9 two-qubit gates for MAJ3 and a circuit with 25 two-qubit gates for MAJ5.

Arbitrary symmetric Boolean functions $f: \{0,1\}^n \rightarrow \{0,1\}$ can also be implemented by signal processing circuits with $O(n^2)$ gates. Suppose without loss of generality that $f(0^n)=0$. We may then let $\phi_x = \frac{\pi}{n+1}|x|$ and find Laurent polynomial coefficients such that $A(\phi_x) = 1-f(x)$, $B(\phi_x) = f(x)$, and derivatives of both $A(\phi)$ and $B(\phi)$ are zero at all points ϕ_x . This leads to $2n+1$ equations and therefore $L = 4n+1$. With A and B constructed this way, once more one can argue that $A(\phi)^2 + B(\phi)^2 \leq 1$.

EXPERIMENTS

Our experiments are executed on qubits Q3, Q5, Q8, Q9, and Q11 of *ibmq_berlin*, a 27-qubit heavy-hexagonal lattice device (Fig. 3). Qubit Q8 is used as the scrap space while Q3, Q5, Q9, and Q11 serve as the input qubits. The measured qubit parameters are shown in Table I below.

Qubit	T1 (μ s)	T2 (μ s)	Readout Error (%)	CNOT (Q _i , Q _j) Error (%)
Q3	108.58	141.83	4.12	(3,5): 0.656
Q5	83.37	109.38	2.24	(5,8): 0.639
Q8	106.08	117.55	1.62	-
Q9	88.57	63.39	1.50	(9,8): 0.720
Q11	126.46	199.23	1.00	(11,8): 0.549

TABLE I. Qubit parameters and CNOT gate errors for the qubits used in the experiment. For the CNOT gate errors, values are measured daily utilizing randomized benchmarking. Parameters were taken from the daily auto-calibration data on July 28, 2020.

Single-qubit gates within our circuits are implemented as standard Qiskit gates comprised of the sequences of $X_{\pi/2}$ rotations and virtual Z rotations [31]. With these two operations, any single-qubit rotation can be realized

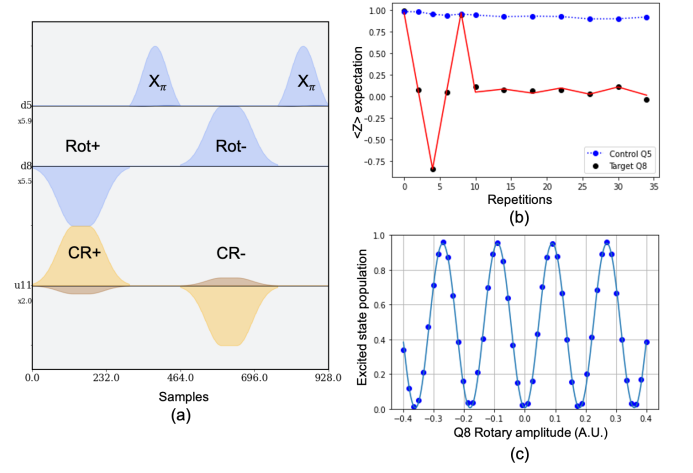


FIG. 4. (a) Pulse diagram of the echoed CR sequence including the rotary echoes applied to the target qubit. The sampling time is 0.2222 ns per sample. “d5” and “d8” denote the drive channels for qubits Q5 and Q8 respectively, while “u12” denotes the cross-resonance channel for the control qubit, Q5. (b) Fine amplitude calibration of the echoed $ZX_{\pi/4}$ CR pulse sequence. Initially the $ZX_{\pi/4}$ pulses are applied in repetitions of 2 to ensure a full rotation about the Bloch sphere. At 16 repetitions, the pulses are applied in repetitions of 4 to apply π pulses about the Bloch sphere equator in order to amplify amplitude errors. (c) Rabi oscillations of the target qubit used to calibrate a 2π rotary echo.

with a maximum of two $X_{\pi/2}$ gates. $X_{\pi/2}$ are implemented applying a 35.5 ns Gaussian microwave pulse at the qubit’s frequency with a Gaussian derivative shaped pulse added to the quadrature phase to reduce leakage out of the computational space. Z rotations are implemented virtually as frame changes within the software by simply shifting the microwave phase of each subsequent microwave pulse by the desired angle of rotation. As a result, single-qubit Z rotations are implemented with essentially no error and they take no time.

The standard two-qubit CNOT gates are implemented using an echoed cross-resonance (CR) drive in which the control qubit is irradiated with a Gaussian-square microwave tone at the target qubit’s frequency (Fig. 4 (a)). The standard echoed CR pulse sequence is as follows: a positive CR tone is applied followed by a π pulse. Then a negative CR tone is applied followed by a second π pulse. The resulting net rotation is $ZX_{\pi/2}$ for the standard CNOT gate. A resonant 2π rotary echo is applied synchronously to the target qubit to minimize cross-talk and unwanted Hamiltonian terms. The phase of the CR drive is calibrated such that the primary interaction term is ZX , relative to the target qubit’s frame. Standard single-qubit and two-qubit gates are auto-calibrated each day. The overall rotation applied is a function of the CR tone amplitude and duration.

To implement custom $\text{CNOT}^{1/2}$ and the locally equiva-

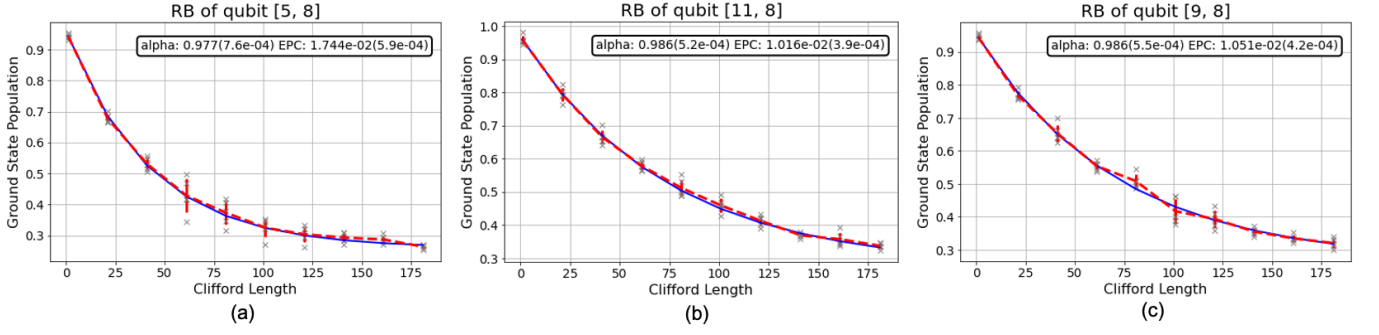


FIG. 5. Randomized benchmarking for decay curves characterizing the $\text{CNOT}^{1/2}$ calibrated in Qiskit Pulse. Pair (Q5, Q8) is shown in (a), (Q11, Q8) in (b), and (Q9, Q8) in (c). Data is shown in red and the fit is shown in blue. Error per Clifford (EPC) is shown in each plot and the error per $\text{CNOT}^{1/2}$ is taken to be $\frac{1}{3}\text{EPC}$.

lent gates we modify the existing CNOT parameters using Qiskit Pulse. The width of the Gaussian-square CR tone is reduced by roughly half and the amplitude is recalibrated such that the amplitude of the custom pulse is roughly equal to the standard CR pulse. In addition, the rotary echo pulse is recalibrated on the target qubit to achieve a 2π rotation within the same duration as the CR tone (Fig. 4 (c)). As the standard CNOT gate CR amplitudes are already optimized to minimize the gate error, our strategy is to maintain this amplitude for the custom CR pulse to minimize gate errors. The net rotation of the custom pulse is thus $ZX_{\pi/4}$, which is equivalent to the custom gates we implement up to the single-qubit gate corrections.

We calibrate the custom CR pulse amplitude by applying repeated echoed $ZX_{\pi/4}$ pulses with the rotary echo and reading out the target qubit along the Bloch sphere equator (Fig. 4 (b)). In this way, amplitude miscalibrations are amplified and can be corrected. Three CR tones are calibrated this way corresponding to the three qubits coupled to the ancilla qubit: (Q5, Q8), (Q9, Q8), and (Q11, Q8).

Once the custom two-qubit gates are calibrated, we measure the error per gate using randomized benchmarking (Fig. 5). We substitute two $\text{CNOT}^{1/2}$ gates for each required CNOT in the Clifford sequence and measure the decay of the $|00\rangle$ population as a function of Clifford gates. From the decay rate, we can extract an error per Clifford gate (EPC). Knowing each Clifford is on average 1.5 CNOT s, and therefore 3 $\text{CNOT}^{1/2}$ s, we can approximate the error rate of the $\text{CNOT}^{1/2}$ as $\frac{1}{3}\text{EPC}$ in the limit of small errors. We extract the $\text{CNOT}^{1/2}$ error rates of 0.00584 ± 0.00019 , 0.00351 ± 0.00014 , and 0.00339 ± 0.00013 for qubit pairs (Q5, Q8), (Q11, Q8), and (Q9, Q8) respectively, which is nearly half the error rate of the standard CNOT for two of the three pairs. Since the dominant error comes from the two-qubit interaction, the error rates of the custom gates (controlled-S, and controlled-HX) are comparable to the measured er-

rors of the $\text{CNOT}^{1/2}$ gate.